Supplemental Materials for Controlling Covalency and Anion Redox Potentials through Anion Substitution in Li-rich Chalcogenides

Andrew J. Martinolich,[†,‖] Joshua J. Zak,[†,‖] David N. Agyeman-Budu,[‡] Seong Shik Kim,[†] Nicholas H. Bashian,[¶] Ahamed Irshad,[§] Sri R. Narayan,[§] Brent C. Melot,[¶] Johanna Nelson Weker,[‡] and Kimberly A. See[*,†]

†*Division of Chemistry and Chemical Engineering, California Institute of Technology, Pasadena, California 91125, United States*

‡*Stanford Synchrotron Radiation Light Source, SLAC National Accelerator Laboratory, Menlo Park, CA 94025, United States*

¶*Department of Chemistry, University of Southern California, Los Angeles, California 90089, United States*

§*Department of Chemistry and Loker Hydrocarbon Research Institute, University of Southern California, Los Angeles, California 90089-1661, United States*

‖*These authors contributed equally to this work*

E-mail: ksee@caltech.edu

Rietveld Refinement Details

Rietveld refinements of powder X-ray diffraction data were executed to gain quantitative structural data regarding the solid solution $Li_2FeS_{2-y}Se_y$. The occupancies of the metals on the mixed Li/Fe site were constrained to 0.5 for both Li and Fe, and the mixed constrained to the input stoichiometry

for the mix ed S/Se site. Positions of the mixed Li/Fe and S/Se sites were allowed to refine and the position of both the Li and the Fe or the S and the Se were forced to remain equivalent. Structural parameters and goodness of fit (reduced χ^2) values are listed in Table S1.

***y* in $Li_2FeS_{2-y}Se_y$**	***a* (Å)**	***c* (Å)**	**reduced χ^2**	**Li_a coordinates (*x*, *y*, *z*)**	**Li_b/Fe coordinates (*x*, *y*, *z*)**	**S/Se position (*x*, *y*, *z*)**
0.2	3.917(1)	6.3248(5)	2.0736	0, 0, 0	1/3, 2/3, 0.337(2)	2/3, 1/3, 0.26(2)
0.6	3.925(2)	6.3949(7)	3.8025	0, 0, 0	1/3, 2/3, 0.35(8)	2/3, 1/3, 0.255(4)
1	3.997(2)	6.4625(5)	3.0625	0, 0, 0	1/3, 2/3, 0.408(6)	2/3, 1/3, 0.224(1)
1.4	4.018(2)	6.5205(5)	4.1616	0, 0, 0	1/3, 2/3, 0.407(3)	2/3, 1/3, 0.234(2)
1.8	4.056(4)	6.5762(5)	7.0756	0, 0, 0	1/3, 2/3, 0.409(1)	2/3, 1/3, 0.227(5)
2	4.058(2)	6.5892(5)	2.5281	0, 0, 0	1/3, 2/3, 0.380(2)	2/3, 1/3, 0.255(1)

Supplemental Figures

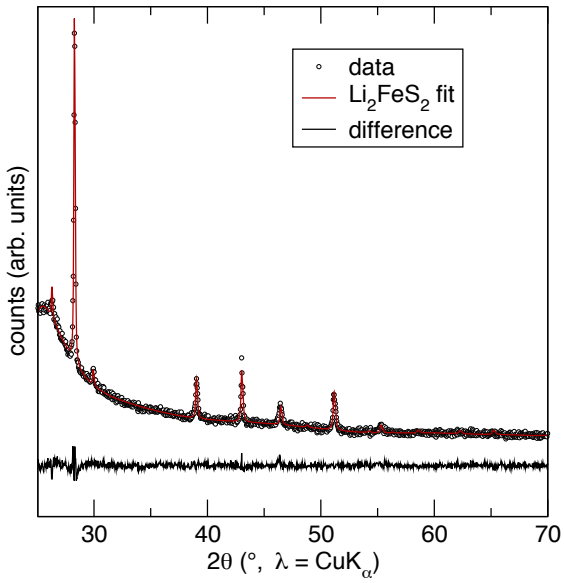

Figure S1: PXRD data and quantitative Rietveld refinement of Li_2FeS_2.

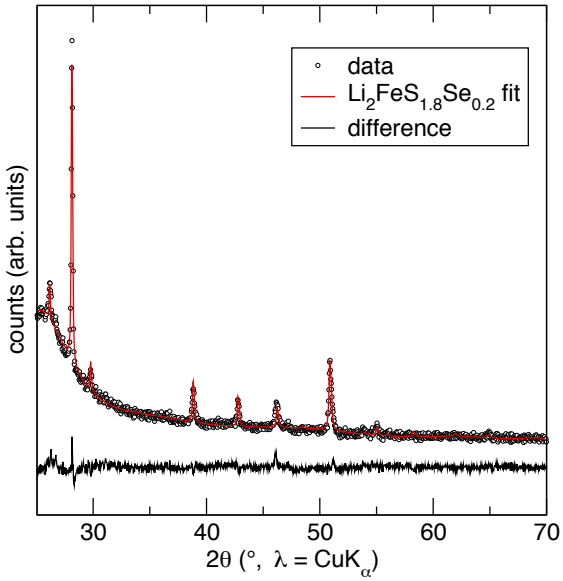

Figure S2: PXRD data and quantitative Rietveld refinement of $Li_2FeS_{1.8}Se_{0.2}$.

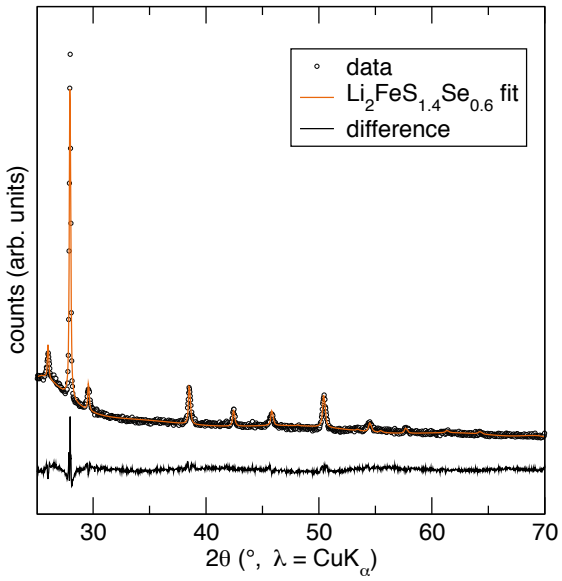

Figure S3: PXRD data and quantitative Rietveld refinement of $Li_2FeS_{1.4}Se_{0.6}$.

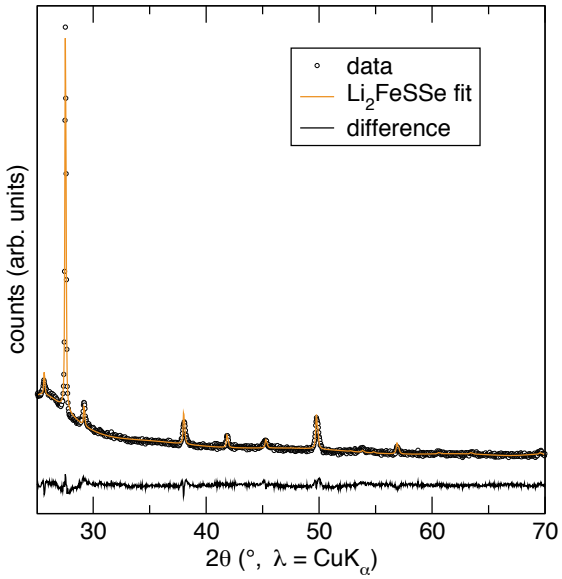

Figure S4: PXRD data and quantitative Rietveld refinement of Li_2FeSSe.

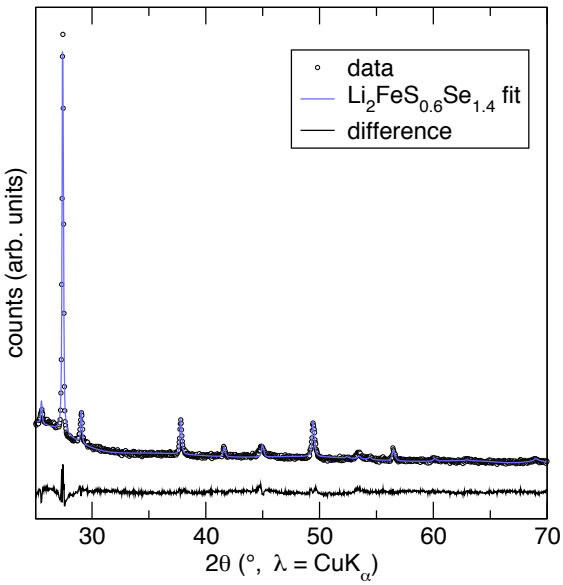

Figure S5: PXRD data and quantitative Rietveld refinement of $Li_2FeS_{0.6}Se_{1.4}$.

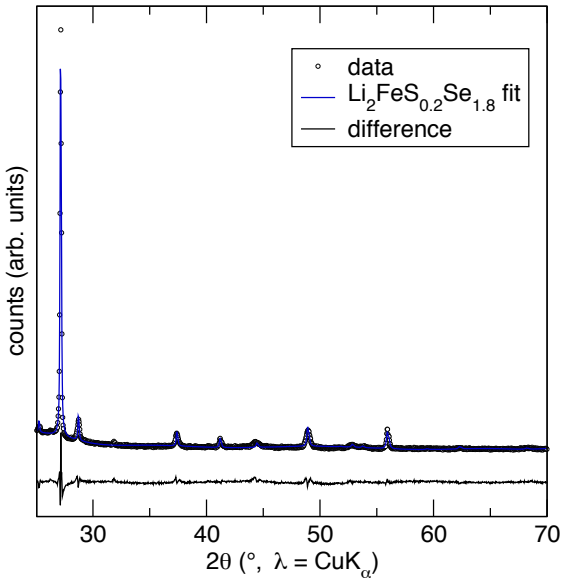

Figure S6: PXRD data and quantitative Rietveld refinement of $Li_2FeS_{0.2}Se_{1.8}$.

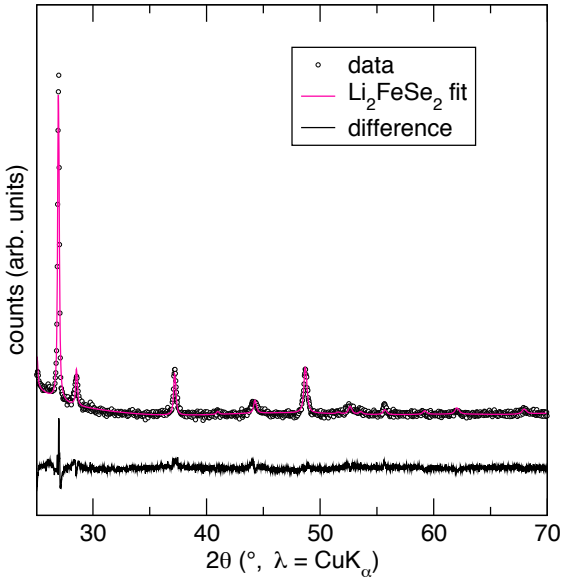

Figure S7: PXRD data and quantitative Rietveld refinement of Li_2FeSe_2.

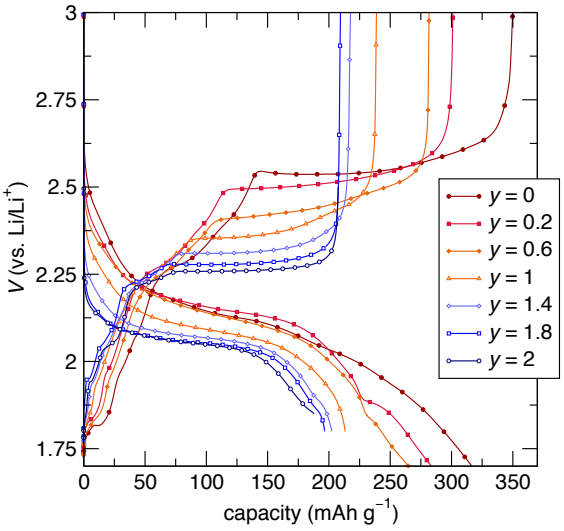

Figure S8: Galvanostatic charge/discharge curves for the solid solution $Li_2FeS_{2-y}Se_y$.

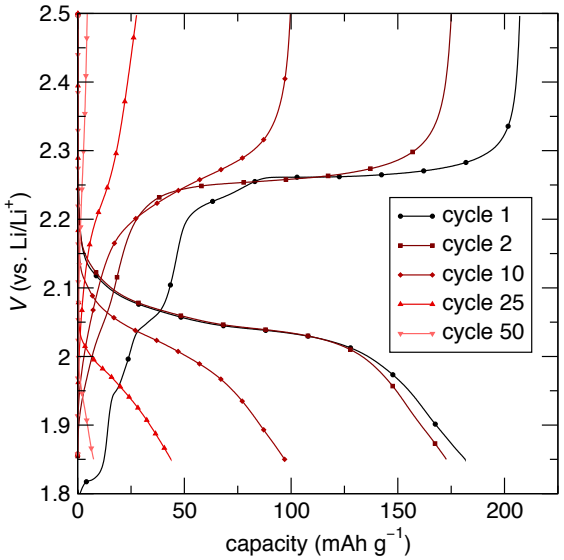

Figure S9: The 1st, 2nd, 10th, 25th, and 50th galvanostatic cycles of Li_2FeSe_2. The first cycle exhibits multiple inflections below 2.25 V, which are not observed upon further cycling. Significant capacity fade occurs in the first 10 cycles.

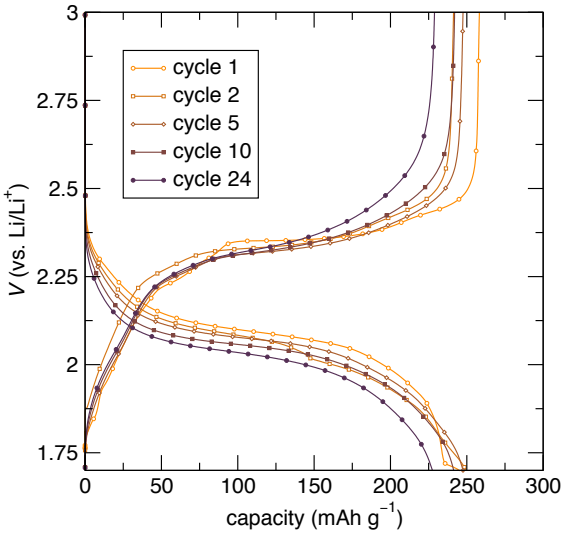

Figure S10: The 1st, 2nd, 5th, 10th, and 24th galvanostatic cycles of Li_2FeSSe. The first cycle exhibits multiple inflections below 2.38 V, which are not observed upon further cycling. Capacity fade becomes evident after the first 10 cycles.

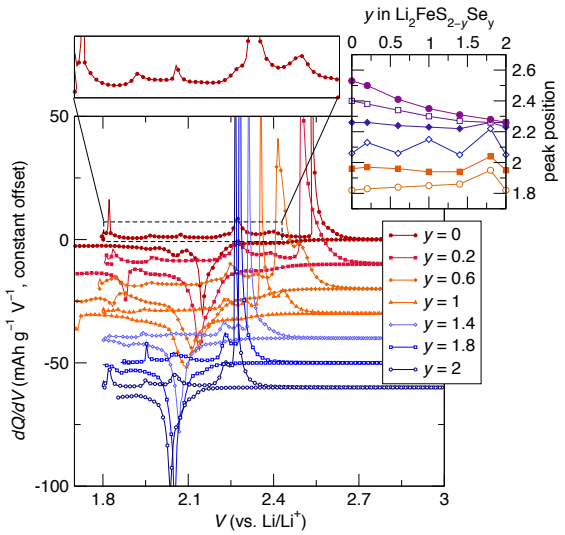

Figure S11: dQ/dV plots of the solid solution $Li_2FeS_{2-y}Se_y$. The inset tracks the various oxidation processes as a function of chalcogen content.

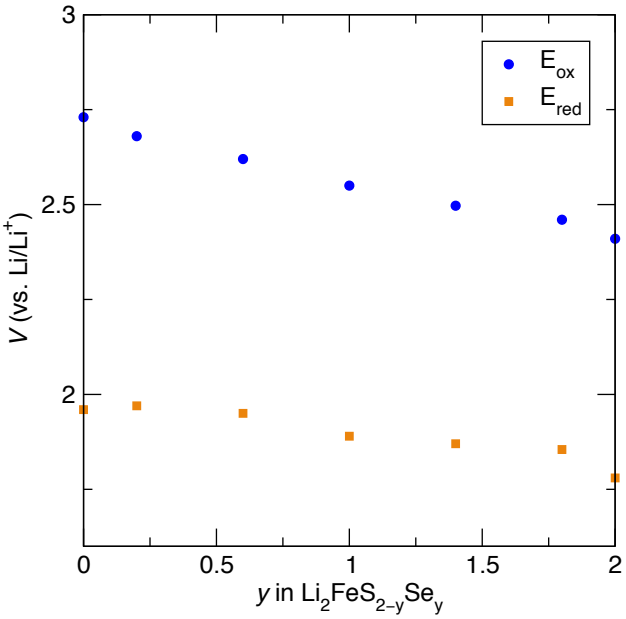

Figure S12: Position of the major oxidative and reductive waves observed via cyclic voltammetry versus chalcogen content.

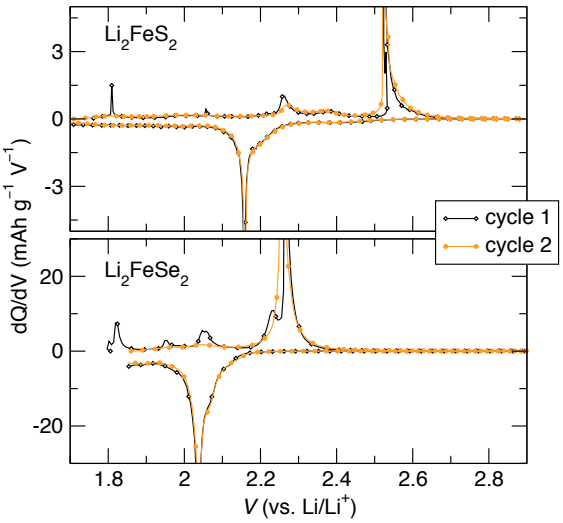

Figure S13: dQ/dV plots of Li_2FeS_2 and Li_2FeSe_2. The sulfide exhibits reproducible electrochemistry from cycle one to cycle two. The selenide exhibits less clear features on the second cycle, indicating some irreversible changes occuring on the first cycle.

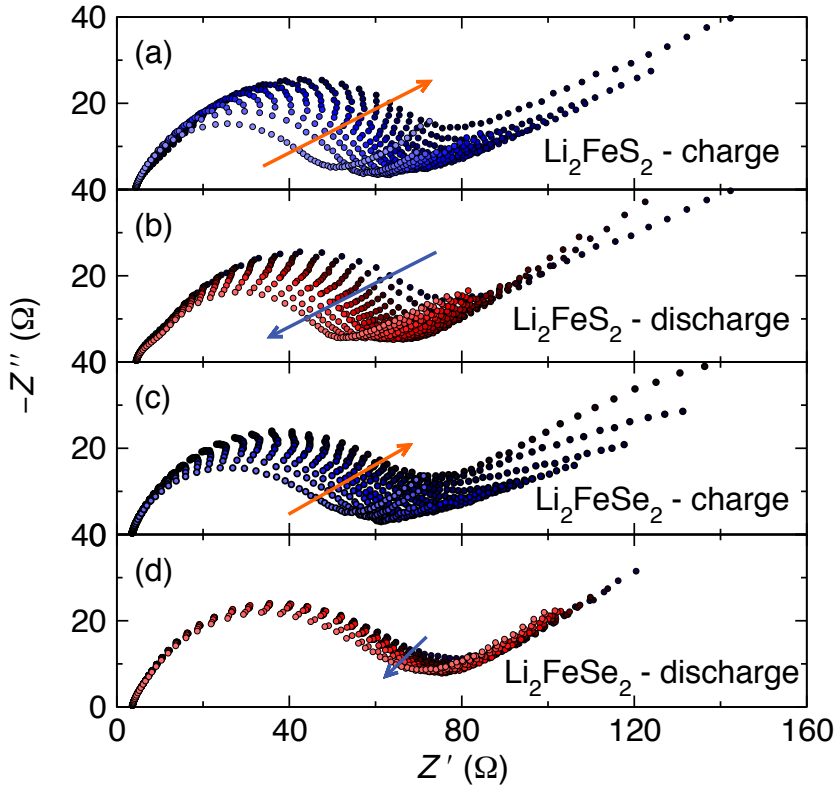

Figure S14: Electrochemical impedance measurements of Li_2FeS_2 and Li_2FeSe_2 cells at various states of charge. While the charge transfer resistance (low frequency, high impedance intercept of the semicircular feature) increases at increasing states of charge for both the sulfide and the selenide, only the sulfide exhibits reversibility and a decrease in the R_{ct} upon discharge.

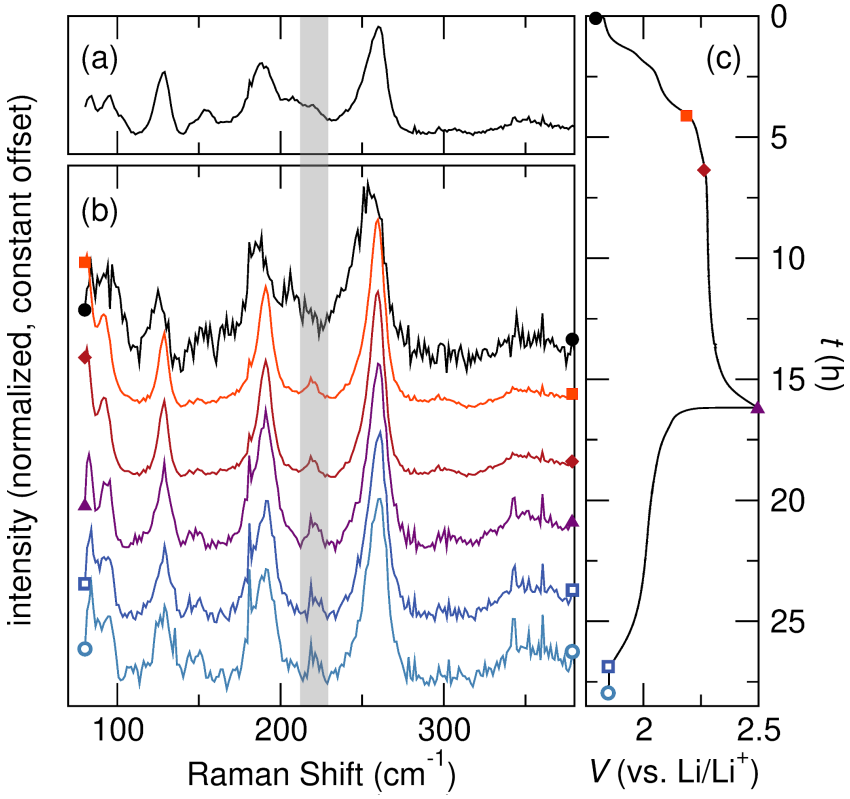

Figure S15: (a) *Ex situ* Raman spectroscopy of pristine Li_2FeSe_2. (b) *In situ* Raman spectroscopy of Li_2FeSe_2 and (c) the correlated charge and discharge curves measured at C/10 based on 1 e^-. A new vibrational mode appears at 219 cm^{-1} appears upon charging and is maintained after the full discharge. The new mode is assigned to Se–Se stretches providing clear evidence of the formation of perselenide moieties throughout the oxidation process as Se and Fe are both oxidized to compensate for Li^+ removal. The perselenide moieties may also be from the new high-impedance phase formed irreversibly during oxidation.